Computational and Structural Biotechnology Journal 18 (2020) 705–713

COMPUTATIONAL AND STRUCTURAL BIOTECHNOLOGY JOURNAL

journal homepage: www.elsevier.com/locate/csbj

A hallmark of phospholamban functional divergence is located in the N-terminal phosphorylation domain

Eli Fernández-de Gortari [a], Rodrigo Aguayo-Ortiz [a], Joseph M. Autry [b,c], L. Michel Espinoza-Fonseca [a,*]

[a] Center for Arrhythmia Research, Department of Internal Medicine, Division of Cardiovascular Medicine, University of Michigan, Ann Arbor, MI 48109, USA
[b] Department of Biochemistry, Molecular Biology, and Biophysics, University of Minnesota, Minneapolis, MN 55455, USA
[c] Biophysical Technology Center, University of Minnesota, Minneapolis, MN 55455, USA

ARTICLE INFO

Article history:
Received 12 November 2019
Received in revised form 23 February 2020
Accepted 23 February 2020
Available online 28 February 2020

Keywords:
Calcium pump
Phospholamban
Sarcolipin
Functional divergence
Phosphorylation domain
Molecular dynamics simulations

ABSTRACT

Sarcoplasmic reticulum Ca^{2+} pump (SERCA) is a critical component of the Ca^{2+} transport machinery in myocytes. There is clear evidence for regulation of SERCA activity by PLB, whose activity is modulated by phosphorylation of its N-terminal domain (residues 1–25), but there is less clear evidence for the role of this domain in PLB's functional divergence. It is widely accepted that only sarcolipin (SLN), a protein that shares substantial homology with PLB, uncouples SERCA Ca^{2+} transport from ATP hydrolysis by inducing a structural change of its energy-transduction domain; yet, experimental evidence shows that the transmembrane domain of PLB (residues 26–52, $PLB_{26–52}$) partially uncouples SERCA *in vitro*. These apparently conflicting mechanisms suggest that PLB's uncoupling activity is encoded in its transmembrane domain, and that it is controlled by the N-terminal phosphorylation domain. To test this hypothesis, we performed molecular dynamics simulations (MDS) of the binary complex between $PLB_{26–52}$ and SERCA. Comparison between $PLB_{26–52}$ and wild-type PLB (PLB_{WT}) showed no significant changes in the stability and orientation of the transmembrane helix, indicating that $PLB_{26–52}$ forms a native-like complex with SERCA. MDS showed that $PLB_{26–52}$ produces key intermolecular contacts and structural changes required for inhibition, in agreement with studies showing that $PLB_{26–52}$ inhibits SERCA. However, deletion of the N-terminal phosphorylation domain facilitates an order-to-disorder shift in the energy-transduction domain associated with uncoupling of SERCA, albeit weaker than that induced by SLN. This mechanistic evidence reveals that the N-terminal phosphorylation domain of PLB is a primary contributor to the functional divergence among homologous SERCA regulators.

1. Introduction

The sarcoplasmic reticulum (SR) Ca^{2+}-ATPase (SERCA) plays a central role in muscle relaxation as it is responsible for translocating Ca^{2+} from the cytosol into the SR of myocytes, thus restoring the SR Ca^{2+} store necessary for subsequent contraction [1]. SERCA activity is regulated by two analogous transmembrane proteins: the 52-residue phospholamban (PLB), which is primarily expressed in ventricles and slow-twitch skeletal muscle, and the 31-residue sarcolipin (SLN), which is predominantly expressed in fast-twitch skeletal muscle and atria [2,3]. PLB and SLN share significant transmembrane domain homology, and both bind to the same canonical M2/M6/M9 groove of SERCA to form 1:1 heterodimeric SERCA–PLB or SERCA–SLN complexes [4–6]. While both regulatory proteins suppress SERCA activity by decreasing the apparent Ca^{2+} affinity of SERCA (K_a), PLB and SLN differ substantially in their mechanisms for SERCA regulation of muscle contractility. Specifically, it has been shown that SLN, but not PLB, contributes to non-shivering thermogenesis in skeletal muscle [7,56] by inducing uncoupling Ca^{2+} transport from ATP hydrolysis by SERCA, thereby stimulating unproductive ATP hydrolysis and heat production [8,9]. Ablation of SLN in mice results in an excessively obese phenotype when fed a high-fat diet, whereas those over-expressing SLN are protected from diet-induced obesity [10]. Conversely, PLB-null mice are not predisposed to diet-induced obesity or glucose intolerance when fed a high-fat diet [11], thus showing that only SLN-induced

Abbreviations: SERCA, sarcoplasmic reticulum Ca^{2+}-ATPase; PLB, phospholamban; SLN, sarcolipin; M4S4, cytosolic extension of transmembrane helix M4; RMSD, root mean square deviation; POPC, 1-palmitoyl-2-oleoyl-*sn*-glycero-3-phosphocholine.

* Corresponding author.
E-mail address: lmef@umich.edu (L. Michel Espinoza-Fonseca).

https://doi.org/10.1016/j.csbj.2020.02.016

uncoupling of SERCA enhances energy expenditure [12]. At the molecular level, it has been shown that SLN, and not PLB, induces unique salt bridge-mediated structural rearrangement of the cytosolic extension of transmembrane helix M4 (M4S4) in the energy-transduction domain of the pump (Fig. S1, Supplemental material) [5,6,13]. This SLN-induced structural change in M4S4 produces a unique structural rearrangement of the gating residue Glu309 that alters occlusion of a Ca^{2+} ion in the transport site II of SERCA and facilitates Ca^{2+} slippage back to the cytosol [13]. This structural change, which is distinct from that required to increase K_a, serves as the primary structural mechanism for SERCA uncoupling by SLN [13]. These studies illustrate the functional and mechanistic differences between PLB and SLN.

There is extensive evidence showing that the functional differences between PLB and SLN lie within the N-terminal segments of these proteins [14]. While there is clear evidence for regulation of SERCA activity by PLB, whose activity is modulated by phosphorylation of its N-terminal phosphorylation domain (residues 1–25,) [15,16], there is less clear evidence for the role of this domain in PLB's functional divergence among homologous SERCA regulators. Specifically, PLB and SLN serve functionally distinct roles in myocytes: PLB binding affects one enzyme parameter (K_a) while SLN controls both K_a and SERCA pumping efficiency (measured as an apparent coupling ratio, Ca^{2+} uptake/ATP hydrolysis [17]). However, opposing evidence has suggested that the isolated transmembrane domain of PLB (residues 26–52, PLB_{26-52}) controls both SERCA's K_a and coupling ratio [18,19]. We have previously shown that PLB and SLN increase K_a by a similar mechanism that involves a highly conserved residue in the transmembrane domain (Asn34 of PLB, analogous to Asn11 of SLN) [20,21]. Conversely, SERCA uncoupling is modulated by two acidic residues in the N-terminus of SLN, Glu2 and Glu7, which form favorable interactions with residues Arg324 and Lys328 of the M4S4 segment of SERCA (Fig. 1) [13]. While these acidic residues are not found in PLB, there are three isosteric polar side chain analogs (residues Gln26, Asn27, and Asn30) in the segment equivalent to the SERCA-uncoupling region of SLN (Fig. 1). Amidated residues are capable of forming stable favorable interactions at protein–protein interfaces [22], e.g., with basic residues Arg or Lys. Thus, the TM domain of PLB may be primarily responsible for SERCA uncoupling, and deletion of the N-terminal phosphorylation domain of PLB may induce structural changes, both allosteric and direct, in the TM domain and/or energy-transduction domain of SERCA to produce PLB-mediated uncoupling (Fig. 1). To systematically test this mechanistic hypothesis and reconcile the seemingly conflicting experimental data on SERCA uncoupling by PLB, we performed five independent 1-μs molecular dynamics simulations (MDS) of the SERCA–PLB_{26-52} complex embedded in a lipid bilayer. The results from these simulations provide novel mechanistic evidence indicating that the N-terminal phosphorylation domain of PLB is a primary contributor to the functional divergence among homologous SERCA regulators [23].

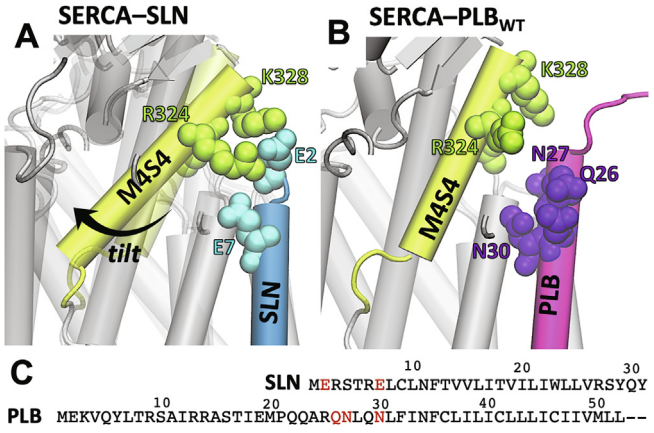

Fig. 1. Structural comparison of M4S4 in SERCA–PLB and SERCA–SLN structures. (A) The SERCA–SLN structure exhibits favorable electrostatic interactions between SLN acidic residue Glu2 and Glu7 in the cytosolic region and SERCA basic residues Arg324 and Lys328 on M4S4; these interactions induce a change in angle the tilt angle of M4S4. (B) In the SERCA–PLB structure, these intermolecular interactions are not present, and no changes are detected in the tilt angle of M4S4 [13]. (C) Alignment of PLB and SLN sequences; residues shown in red are important for SLN-mediated uncoupling or hypothesized here to play a role in PLB-mediated SERCA uncoupling. Proteins are shown in gray cartoon representation, and key residues are shown as spheres. (For interpretation of the references to colour in this figure legend, the reader is referred to the web version of this article.)

2. Materials and methods

2.1. Setting up the SERCA–PLB_{26-52} system

We used an atomic model of the full-length PLB bound to SERCA generated previously by our group [21] to simulate the binary complex of SERCA bound to the isolated transmembrane domain of PLB, PLB_{26-52}, at physiological conditions. To this aim, we deleted the cytosolic N-terminal phosphorylation domain of PLB (residues 1–25). We modeled transport site residues Glu309, Glu771 and Asp800 as unprotonated and residue Glu908 as protonated. In addition, we adjusted the pK_a of other ionizable residues to a pH value of ~7.2 using PROPKA 3.1 [24,25]. The complex was inserted in a pre-equilibrated 120 × 120 Å bilayer of POPC lipids. We used the first layer of phospholipids that surround SERCA [26] as a reference to insert the complex in the lipid bilayer. This initial system was solvated using TIP3P water molecules with a minimum margin of 15 Å between the protein and the edges of the periodic box in the *z*-axis. K^+ and Cl^- ions were added to produce a KCl concentration of approximately 100 mM.

2.2. Molecular dynamics simulations

MDS of all systems were performed by using the program NAMD [27] with periodic boundary conditions [28], particle mesh Ewald [29,30], a non-bonded cutoff of 12 Å, and the RATTLE algorithm to constrain bonds to hydrogen atoms and allow a 2 fs time step. CHARMM36 force field topologies and parameters were used for the proteins [31], lipid [32], water, K^+ and Cl^-. The NPT ensemble was maintained with a Langevin thermostat (310 K) and an anisotropic Langevin piston barostat (1 atm). Solvated systems were first subjected to energy minimization, followed by gradually warming up of the systems for 200 ps. This procedure was followed by 20 ns of equilibration with backbone atoms harmonically restrained using a force constant of 10 kcal mol^{-1} $Å^{-2}$. Given the size of the systems, we assigned random initial velocities to atoms that match the desired temperature is achieved to produce independent simulations; these structures are then used as a starting point for the production MD simulations. We performed five independent 1-μs MD replicates of SERCA–PLB_{26-52} to obtain statistical significance.

2.3. MD trajectories of SERCA–PLB and SERCA–SLN

Microsecond-long, independent trajectories of the complexes between wild-type PLB (six trajectories) and SLN (five trajectories) reported by our group were used in this study [21,33,34]. We take advantage of these trajectories because they were performed under lipid and ion composition, box size (this variable might affect adequate sampling of structural states [35]), temperature, and pressure that are similar to those used in this study. Therefore,

these published trajectories represent well-characterized MD replicates that are sufficiently robust to obtain statistical significance.

2.4. Structural analysis

We calculated the fraction of native inhibitory contacts (Q_{inh}) between transmembrane PLB residues Leu31, Asn34, Phe35 and Ile38 and SERCA [33] to measure the effect of Ca^{2+} binding on the stability of the interface between SERCA and wild-type PLB or $PLB_{26–52}$. For this analysis, we focused only on these residues because the inhibitory activity of PLB is primarily localized in the transmembrane domain [19,57–62], and because a decrease in Q_{inh} involving these PLB residues directly correlates with relief of SERCA inhibition [33]. Based on a previous study by our group, Q_{inh} is defined by a list of native contact pairs (i,j) in the crystal structure of the complex. All pairs of heavy atoms i and j belonging to residues Ai and Aj are in contact if the distance between i and j is <7 Å [33]. Q_{inh} is expressed as a number between 1 and 0, and it is calculated as the total number of native contacts for a given time frame divided by the total number of contacts in the crystal structure of the SERCA–PLB complex (PDB code: 4kyt) [4].

We calculated the tilt angle for M4S4 for each independent trajectory, relative to M4S4 in the crystal structure of PLB-inhibited SERCA; the tilt angles for each set of independent MDS were then combined into a single histogram. Finally, each histogram was fitted to either one-Gaussian or two-Gaussian distance distributions $\rho(R)$. To express the two-Gaussian model, we used the following fitting model:

$$\rho(R) = \sum_{j=1}^{2} X_j \sigma_j^{-1} (2\pi)^{-1/2} \exp - \left[(R - R_j)/(2\sigma_j)\right]^2,$$

$$\sigma_j = \mathrm{FWHM}_j / \left[2 * (2\ln 2)^{1/2}\right]$$

where R_1 and R_2 are the centers of each structural state; $FWHM_1$ and $FWHM_2$ are the full widths at half maximum for each distribution; and X_1 and X_2 are the relative mole fractions of each structural state.

2.5. Statistical analysis

Data are reported as the mean ± SE. For comparison between groups, a student's t-test was performed. A p-value <0.05 was taken as significant.

3. Results and discussion

We measured time-dependent root-mean square deviation (RMSD) changes of $PLB_{26–52}$ in the complex, as well as change in the RMSD of the cytosolic and transmembrane domains of SERCA to determine if $PLB_{26–52}$ forms a stable complex with SERCA that retains the structural and functional features similar to those of the wild-type PLB (PLB_{WT}) at physiological conditions. RMSD plots show that the position of $PLB_{26–52}$ in the binding groove of SERCA in all five trajectories does not deviate substantially (e.g., RMSD <2.5 Å) from the initially bound structure of the complex (Fig. S2, Supplemental material). Complementary evaluation of the time-dependent changes in the secondary structure show that $PLB_{26–52}$ folds as a stable α-helix, with an average helical content of 97 ± 3% (n = 5); this fold is virtually identical to that observed for the same residues in PLB_{WT} bound to SERCA (α-helical content = 98 ± 2%, n = 6) [21]. These findings indicate that deletion of the cytosolic segment is not required for the structural stability of the transmembrane helix of PLB, in qualitative agreement with previous reports [21,36,37]. In the presence of bound PLB_{WT}, the cytosolic headpiece of SERCA is inherently mobile, and that relief of SERCA inhibition produces a dynamically ordered structure of the headpiece [38]. Therefore, we asked whether the global dynamic properties of SERCA are altered in the presence of $PLB_{26–52}$. We found that the transmembrane domain of SERCA does not deviate substantially from the initial structure in solution, whereas the cytosolic headpiece that is exposed to the aqueous phase is structurally dynamic in solution (e.g., in trajectories 1, 3, and 5; Fig. S2, Supplemental material). These findings suggest that $PLB_{26–52}$ forms a stable complex with the canonical binding site of SERCA, and also indicate that the structural dynamics of the complex is similar to that observed in the SERCA–PLB_{WT} complex [21].

While $PLB_{26–52}$ remains bound to the canonical site of SERCA, it is possible that removal of the N-terminal phosphorylation domain facilitates the formation of non-native SERCA–PLB intermolecular contacts, thus explaining $PLB_{26–52}$-induced [19] uncoupling of SERCA. We measured the relative tilt angle and the displacement along the membrane normal (z axis) of $PLB_{26–52}$ using the crystal structure of SERCA–PLB as a reference (Table 1). These parameters were compared to those calculated for residues 26–52 of PLB in six independent trajectories of the SERCA–PLB_{WT} complex to quantitatively determine the changes in orientation of $PLB_{26–52}$. We found that $PLB_{26–52}$ helix exhibits on average a 0.3° change in the tilt angle relative to the position of PLB in the crystal structure of the complex (Table 1). Similarly, we found that, on average, $PLB_{26–52}$ undergoes a 1 ± 0.4 Å displacement along the membrane normal toward the cytosolic side of the membrane; this value is very similar to that found in the SERCA–PLB_{WT} complex (0.8 ± 0.1 Å, Table 1). While these findings indicate that $PLB_{26–52}$ undergoes changes in its orientation relative to the crystal structure of the complex, we found no significant differences in either tilt angle or axial displacement between $PLB_{26–52}$ and PLB_{WT} bound to SERCA in the μs time scale. A complementary metric we use here to evaluate the stability of the SERCA–$PLB_{26–52}$ complex is the fraction of native inhibitory contacts, Q_{inh}, between the Ca^{2+}-free SERCA and PLB residues Leu31, Asn34, Phe35 and Ile38 (Fig. S3, Supplemental material). We chose these residues because they are in direct contact with SERCA, because they are known to play a role in increasing K_a of SERCA [39–41], and because changes in Q_{inh} for these residues serve as a proxy for identifying Ca^{2+}-induced relief of pump inhibition in the SERCA–PLB regulatory complex [33]. Analysis of the Q_{inh} values showed that in comparison with the SERCA–PLB_{WT} complex, $PLB_{26–52}$ retains a substantial fraction of native-like contacts with SERCA (e.g., $Q_{inh} \geq 0.65$) (Table 1). We detected a loss in the fraction of native contacts of some PLB residues in the trajectories of the SERCA–$PLB_{26–52}$ complex (Table 1). Here, we found that Asn34 and Ile38 of $PLB_{26–52}$ show the largest difference in Q_{inh} values compared with the native SERCA–PLB_{WT} complex (e.g., average ΔQ_{inh} values of 0.06 ± 0.08 and 0.11 ± 0.07, respectively). However, the Q_{inh} values for these residues are not significantly different between SERCA–$PLB_{26–52}$ and SERCA–PLB_{WT}, which indicates that deletion of the N-terminal phosphorylation domain does not affect local intermolecular interactions involving key residues required for PLB inhibition of SERCA.

To further assess if $PLB_{26–52}$ forms native-like inhibitory contacts with SERCA, we determined whether the structural changes within the transport sites induced by $PLB_{26–52}$ correspond to those induced by PLB_{WT}. PLB inhibits SERCA by inducing a spatial separation between residues Glu771–Asp800, Glu771–Glu908 and Asp800–Glu908, thus blocking binding of metal ions in site I and inhibiting the formation of the Ca^{2+}-activated state of the pump [4,21,33]. We found that binding of $PLB_{26–52}$ induces similar spatial separation between residues Glu771, Asp800 and Glu908 as those found in the native complex in either crystal environment (PDB: 4kyt) [4] (Fig. 2) or in solution [21]. We found that the distance between residues Glu771 and Asp800 is substantially longer than

Table 1
Effects of deletion of the N-terminal phosphorylation domain of PLB on the topology of the transmembrane helix and the inhibitory SERCA–PLB contacts.

Complex	Tilt angle (°)[a,b]	Displacement along the *z* axis (Å)[a,b]	Fraction of native contacts, Q_{inh}[a,b,c]			
			Leu31	Asn34	Phe35	Ile38
SERCA–$PLB_{26–52}$	4.0 ± 0.8	1.0 ± 0.4	0.67 ± 0.07	0.68 ± 0.07	0.65 ± 0.08	0.67 ± 0.06
SERCA–PLB_{WT}[d]	3.7 ± 0.8	0.8 ± 0.1	0.68 ± 0.05	0.74 ± 0.04	0.63 ± 0.06	0.78 ± 0.03

[a] Values reported as mean ± SE for all the trajectories combined; n = 5 for SERCA–$PLB_{26–52}$, and n = 6 for SERCA–PLB_{WT}. There is no statistically significant difference between the control (SERCA–PLB_{WT}) and the designed (SERCA–$PLB_{26–52}$) groups ($p < 0.05$).
[b] Relative to the transmembrane domain of PLB in the inhibited SERCA–PLB crystal structure (PDB: 4kyt) [4].
[c] Mutation of this residue to alanine partially reverses PLB-induced increase in K_a [39–41].
[d] MD trajectories reported in previous studies of the inhibited, full-length SERCA–PLB_{WT} complex [21,33,34].

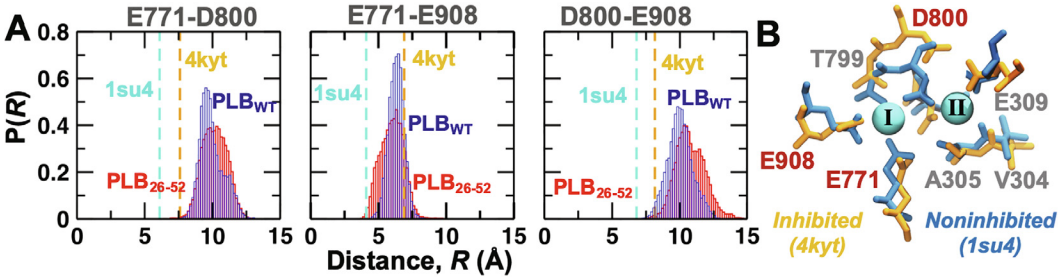

Fig. 2. PLB_{WT} and $PLB_{26–52}$ inhibit Ca^{2+} affinity of SERCA by controlling coordination geometry in transport site I. (A) Distance distribution between SERCA residue pairs Glu771–Asp800, Glu771–Glu908, and Asp800–Glu908 in transport site I were calculated from the combined trajectories for SERCA–PLB_{WT} (blue) or SERCA–$PLB_{26–52}$ (red); in all cases, the distance was calculated between the carboxylic groups of each amino acid pair. The dashed cyan line shows the atom–atom distance when transport site I adopts a competent geometry for Ca^{2+} binding, as observed in the crystal structure of SERCA (PDB: 1su4) [55]; the dashed orange line indicates the atom–atom distance when transport site I adopts an inhibited geometry, as detected in crystal structure of SERCA–PLB (PDB: 4kyt) [4]. (B) Crystal structures and Ca^{2+} interactions with the transport sites of SERCA. This figure illustrates the location of Ca^{2+} ions (cyan spheres) and the structural arrangement of the residues that bind Ca^{2+} in the Ca^{2+}-activated (or noninhibited) state of the pump (blue sticks). For comparison, we show the structural arrangement of the transport sites as populated in the inhibited state of the SERCA–PLB complex (orange sticks). Based on the structural characteristics of each configuration, the transport sites are classified as inhibited or not inhibited. Here we find that deletion of PLB's N-terminal phosphorylation domain does not reverse changes in the transport site I associated with increase in K_a. (For interpretation of the references to colour in this figure legend, the reader is referred to the web version of this article.)

that found in both the Ca^{2+}-bound and PLB-bound SERCA complexes; this observation is important because we have recently shown that these residues come closer to each other during the early formation of competent Ca^{2+} transport sites [33]. Together, these findings demonstrate that in the absence of the cytosolic domain, $PLB_{26–52}$ adopts structural arrangement and forms inhibitory intermolecular contacts with SERCA that are similar to those found in the native SERCA–PLB_{WT} complex, in agreement with experiments showing that the isolated transmembrane domain of PLB alters K_a of SERCA in a reconstituted membrane system [18]. Furthermore, the high alpha-helix structural stability of $PLB_{26–52}$ and the inability of its cytosolic segment to undergo order-to-disorder transitions in the μs timescale also provides a mechanistic explanation for the inhibitory potency retained by the isolated transmembrane domain of PLB [36].

After establishing that SERCA–$PLB_{26–52}$ complexes are stable at physiological conditions and that $PLB_{26–52}$ retains its inhibitory activity against SERCA, we evaluated whether PLB residues Gln26, Asn27, and Asn30 form favorable interactions with residues Arg324 and Lys328 of SERCA. We chose these PLB residues because of their spatial proximity to Arg324 and Lys328 of SERCA, which play a key role in the mechanism for SERCA uncoupling by SLN [13]. Distance distributions showed that in the SERCA–PLB_{WT} complex, Gln26 of PLB interacts Arg324 of SERCA (via contacts $R \leq 7$ Å between heavy atoms [42], Fig. 3). These interactions account for 82% of the intermolecular distances sampled over the total simulation time (t_{total} = 6 μs). We found that the short-range interaction between Gln26 and Arg324 is also present in the SERCA–$PLB_{26–52}$ complex, albeit at lower fraction (60%) over the course of five independent 1-μs trajectories (Fig. 3A). A similar shift in the residue-residue distance distributions was observed between PLB residue Asn30 (analogous position as SLN Glu7, the key SERCA-uncoupling residue [13]) and SERCA residue Arg324. Here, the fraction of short-range interactions decreases from 31% to 11% upon deletion of PLB's N-terminal phosphorylation domain (Fig. 3A). We found that residue pairs $Gln26^{PLB}$–$Lys32^{SERCA}$ and $Asn27^{PLB}$–$Lys328^{SERCA}$ do not interact in the SERCA–PLB_{WT} complex. However, deletion of PLB's N-terminal phosphorylation domain induces a shift in the distance between Gln26/Asn27 of PLB and Lys328 of SERCA. Specifically, $Gln26^{PLB}$–$Lys328^{SERCA}$ becomes on average 5 Å shorter in the SERCA–$PLB_{26–52}$ complex, and the fraction of short-range intermolecular distances increases to 6% (Fig. 3); the fraction of short-range contacts in $Ans27^{PLB}$–$Lys328^{SERCA}$ accounts only for 1.5% of the intermolecular distances sampled over the total simulation time (t_{total} = 5 μs). Together, these findings indicate that the N-terminal phosphorylation domain of PLB controls intermolecular contacts involving the energy-transduction domain of SERCA. These findings are important because (i) SERCA residues Arg324 and Lys328 play key roles in modulating the orientation of M4S4 that favor uncoupling of the pump [13]; (ii) PLB residue Gln26 is highly conserved (Fig. S4, Supplemental material); (iii) human PLB, which encodes Lys27, is ~1.4 fold more potent inhibitor than rabbit PLB, and (iv) mutation of Asn27 to alanine (Asn27Ala) or aspartate (Asn27Asp) induces gain and loss of inhibition, respectively [43].

We measured the effects of $PLB_{26–52}$, PLB_{WT} [21,33,34] and SLN [13,21] on the structural arrangement of M4S4 to evaluate the effects of PLB's N-terminal phosphorylation domain on the structural changes associated with SERCA uncoupling. Specifically, we calculated the axial tilt angle of M4S4 in SERCA complexes relative to the SERCA–PLB crystal structure [4] for each system combined, and then constructed probability histograms for each SERCA-bound complex. Each histogram was then fitted to a Gaussian distribution model; we tested a one-Gaussian distribution and

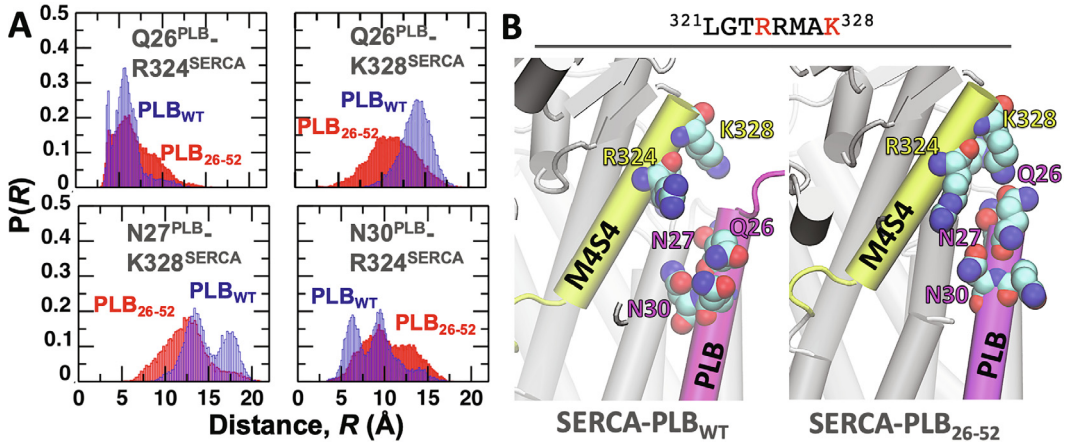

Fig. 3. Distance distributions between PLB residues Gln26, Asn27, and Asn30 and SERCA residues Arg324, and Lys328. (A) Distance distribution histograms were calculated for the amino acid pairs $Gln26^{PLB}$–$Arg324^{SERCA}$, $Gln26^{PLB}$–$Lys328^{SERCA}$, and $Asn30^{PLB}$–$Arg324^{SERCA}$; intermolecular distances for the SERCA–PLB^{WT} and SERCA–$PLB_{26–52}$ complexes are shown in blue and red, respectively. The distance between residue pairs was calculated between the oxygen atom from the carboxylamine group of Asn/Gln and the N_ζ and C_ζ atoms of Lys and Arg, respectively. (B) Representative structures showing the interaction between M4S4 of SERCA (yellow) and PLB_{WT} or $PLB_{26–52}$ (magenta) obtained from MD trajectories. Residues of SERCA and PLB studied here are shown as spheres. Sequence of M4S4 is shown; residues Arg324 and Lys328 are in red. (For interpretation of the references to colour in this figure legend, the reader is referred to the web version of this article.)

two-Gaussian distributions (See Section 2). As exemplified in Fig. 4, the two-component is superior for the PLB-bound complexes, with χ^2 values about 2–3 times less than for one-component models (Table S1, Supplemental material). Conversely, the single-component model was selected for the SERCA–SLN complex because it avoids overfitting of the model (e.g., by marginally minimizing χ^2 through adding an additional parameter; Table S1, Supplemental material), and because it is also consistent with reported data [13].

In the SERCA–SLN complex, the tilt angle of M4S4 fits to a one-Gaussian distribution with center at 18.2° (Fig. 4, *green* trace) and FWHM of 5.8° (Table S2, Supplemental material). These findings do not support the presence of a tilted, more dynamic structure of the M4S4 domain. The average tilt angle populated in the MD trajectories is in good agreement with the 17° tilt angle of M4S4 calculated using the crystal structures of SERCA–SLN [5,6]. In contrast to the SERCA–SLN complex, we found that fitting of the M4S4 tilt angle histogram to a two-Gaussian distribution for the SERCA–PLB_{WT} complex yields two populations: a predominantly populated structural state with center at 2.5°, and a structural state at 7° (Fig. 4A, *purple and magenta traces, respectively*). Unlike SERCA–SLN, we found that both tilt angle distributions of M4S4 in the SERCA–PLB_{WT} complex are narrow, with $FWHM_1$ and $FWHM_2$ values of 3.3° and 4.2° , respectively (Table S2, Supplemental material). We found that removal of PLB's N-terminal phosphorylation domain also produces two structural states with centers at 3.2° and 6.9° (Fig. 4B, *purple and magenta traces, respectively*), but induces a substantial redistribution of the structural states of M4S4. Specifically, binding of $PLB_{26–52}$ decreases the fraction of the M4S4 population at R_1 = 3.2° by 20%, and shifts the equilibrium toward a distribution at R_2 = 6.9° (Fig. 4B, *magenta trace*). Most important, we found that binding of $PLB_{26–52}$ to SERCA produces a broader ($FWHM_2$ = 6.4°) distribution of the population with center at 6.9°. These structural changes indicate that compared to PLB_{WT}, binding of $PLB_{26–52}$ to SERCA gives rise to a more tilted and dynamically disordered structure of the M4S4 domain. While these structural changes are weaker than those induced by SLN, the shift toward a dynamically disordered M4S4 provides a mechanistic explanation for the partial uncoupling of SERCA observed in reconstituted vesicles [19]. These findings also provide novel insights into the mechanisms for SERCA uncoupling. Specifically, we have recently shown that under wild-type conditions (e.g., SERCA bound to full-length PLB), the M4S4 domain of SERCA is not in equilibrium between tilted and not tilted structures, and that only SLN binding induces a change in the tilt angle that correlates with uncoupling of the pump. While our current study does not contradict this mechanism, it demonstrates that changes in tilt of M4S4 does not simply work as an 'on/off' switch, and that regulation/uncoupling of the pump is a fine-tuned process.

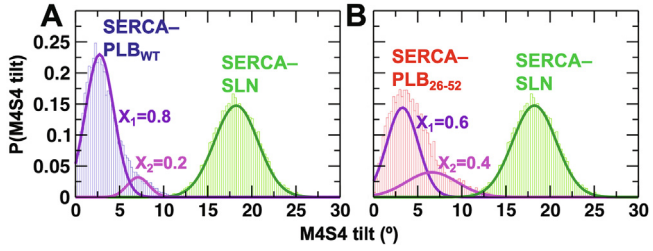

Fig. 4. Tilt angle distributions of the energy-transduction M4S4 domain of SERCA. (A) M4S4 tilt angle distributions determined by MDS for the complex between SERCA and PLB_{WT} (blue bars) or SLN (green bars). (B) M4S4 tilt angle distribution calculated using independent MD trajectories combined of the SERCA–$PLB_{26–52}$ (red bars) complex and SERCA–SLN (green bars). In both SERCA-PLB_{WT} and SERCA–$PLB_{26–52}$, two structural populations are resolved at 2.5–3.2° (purple trace) and at 6° (magenta trace). X_1 and X_2 are the relative mole fractions calculated for each tilt angle-based structural population of M4S4. (For interpretation of the references to colour in this figure legend, the reader is referred to the web version of this article.)

We ask whether changes in SERCA–PLB distance distributions induced by deletion of PLB's N-terminal phosphorylation domain explain changes in the tilt angle distributions of M4S4 that induce uncoupling of the pump. Therefore, we calculated the Pearson's correlation coefficient to measure the strength of a linear association between intermolecular distances and the relative M4S4 tilt angle populated in the SERCA–$PLB_{26–52}$ complex. Except for $Asn27^{PLB}$–$Lys328^{SERCA}$, there is a weak positive linear relationship (Pearson's r between 0.20 and 0.25, Fig. 5) [44] between the SERCA–PLB intermolecular distances reported in Fig. 3 and the tilt angle of M4S4. Based on these observations, it is possible that there is no causal relationship between SERCA–PLB intermolecular distances and the relative M4S4 tilt angle in the SERCA-$PLB_{26–52}$ complex. However, we found that in the SERCA–PLB_{WT} complex, the correlation between SERCA–PLB intermolecular distances and the

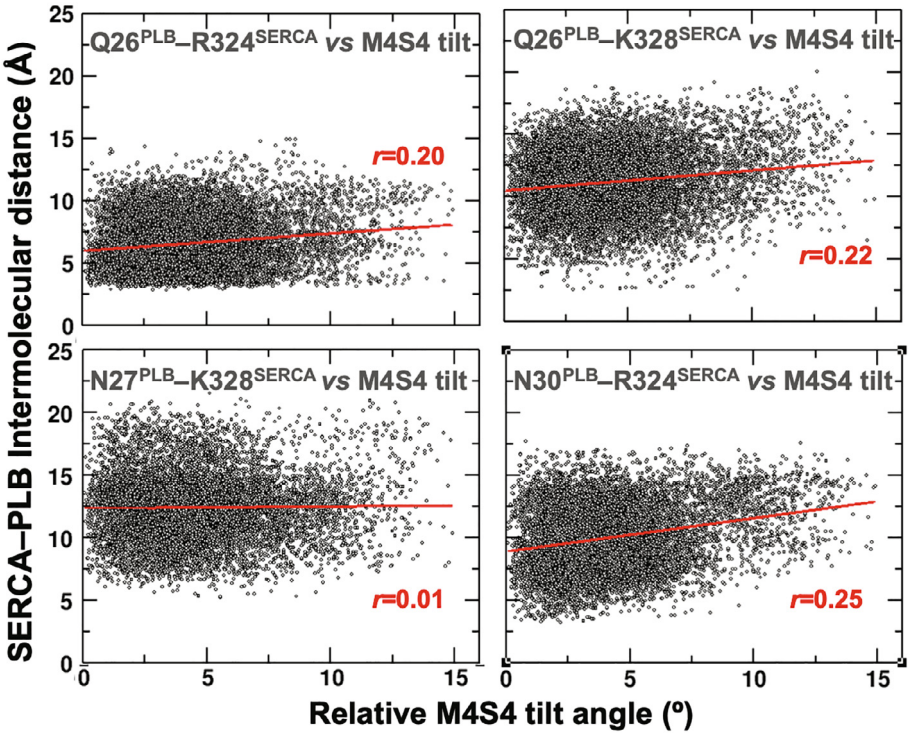

Fig. 5. Moderate correlation between SERCA–PLB intermolecular distances and the M4S4 tilt angle for the complex between SERCA and $PLB_{26–52}$. Each point represents a single structure extracted at time intervals of 400 ps.

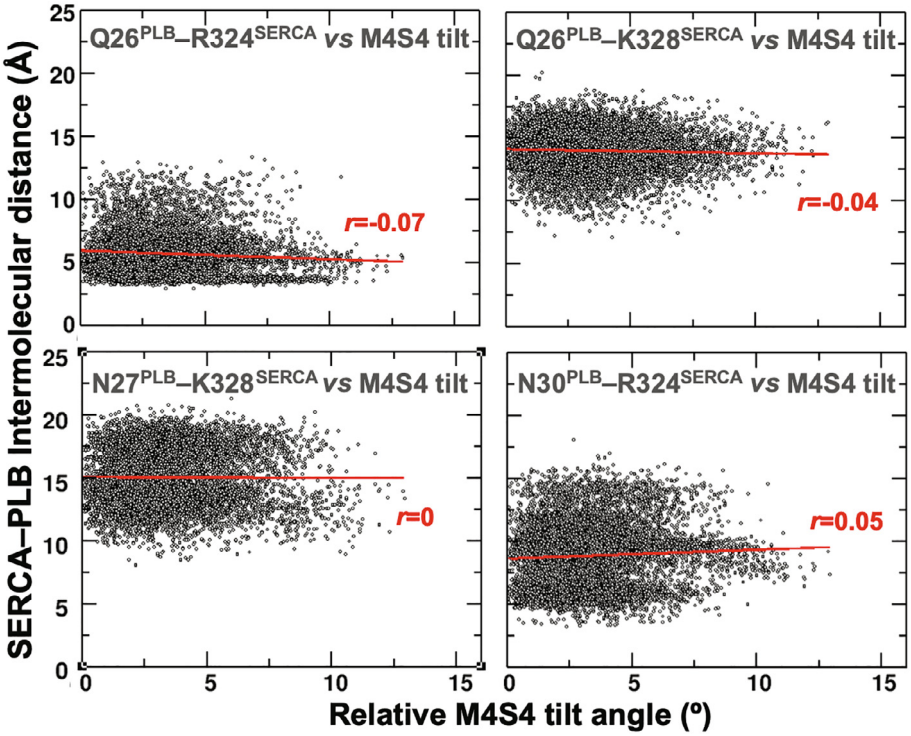

Fig. 6. Lack of correlation between SERCA–PLB intermolecular distances and the M4S4 tilt angle for the complex between SERCA and PLB_{WT}. Each point represents a single structure extracted at time intervals of 400 ps.

M4S4 tilt angle is negligible (i.e., *r* values between −0.07 and 0.05 [44]; Fig. 6). These findings are significant because they suggest that that upon deletion of PLB's N-terminal phosphorylation domain, changes in the distances between PLB residues Gln26 and Asn30 and SERCA residues Arg324 and Lys328 contribute to the changes in the orientation and dynamics of M4S4 that induce partial uncoupling of the pump. While a weak correlation suggests that other factors might contribute to the structural change in M4S4 (e.g., intradomain communication), these findings support the notion that PLB's N-terminal phosphorylation domain exerts

control on the structural dynamics of the energy-transduction domain of SERCA. Here, the phosphorylation domain of PLB imposes constraints on SERCA's energy-transduction domain, and its deletion results in a redistribution of structural states that produces a mobile M4S4 domain. As a results of these changes, SERCA likely populates a dynamically disordered Ca^{2+} site II that that perturbs optimal Ca^{2+} occlusion by the gating residue Glu309 [45–47] and thus facilitates Ca^{2+} slippage back to the cytosol and uncoupling of the pump (Fig. 7). This mechanism for $PLB_{26–52}$ uncoupling of SERCA is consistent with the alternating electrostatic interactions between SERCA and SLN, which produce a dynamically disorder M4S4 in solution [13]. These findings are also in line with the concept that relatively small structural changes are sufficient to induce substantial changes in the function of proteins [48–51]. This mechanistic data explains previous observations [19], and indicates that PLB's N-terminal phosphorylation domain is required for the functional divergence among homologous SERCA regulators.

Do additional mechanisms play a role in $PLB_{26–52}$ uncoupling of SERCA? We proposed three alternative hypotheses: (1) *Formation of a higher-order SERCA/PLB complex*: SERCA uncoupling by $PLB_{26–52}$ was observed at high PLB:SERCA molar ratios [19]; a recent study showed that at such molar ratios, PLB_{WT} plays a distinct structural and functional role in SERCA regulation [52]. Here, PLB oligomerizes into pentamers, interacts with transmembrane segments M3 of SERCA, and stimulate SERCA's ATPase activity [52]. Therefore, the formation of higher order SERCA/$PLB_{26–52}$ might explain the partial uncoupling function of $PLB_{26–52}$ detected *in vitro*. (2) *Control of M1 helix of SERCA*: previous reports have suggested that protein–protein interactions involving M1 of SERCA might result in the uncoupling of the pump [14]. However, we found no evidence that $PLB_{26–52}$ directly interacts with helix M1. These findings are in line with previous crystallographic [5,6] and computational [13] analyses showing that uncoupling of SERCA is directly linked to changes in the orientation and dynamics of M4S4. (3) *Structural changes of the transport sites:* it is possible that truncation of the N-terminal phosphorylation domain induces uncoupling of SERCA through a mechanism that depends on regulation of K_a. However, we found that $PLB_{26–52}$ and SLN produce a transport site geometry associated with inhibition [21] that is very similar to that produced by PLB_{WT} (Fig. 2), while inducing changes in the structural tilt angle of M4S4. These findings suggest that modulation of Ca^{2+} affinity is independent from the structural changes in M4S4 induced by $PLB_{26–52}$, in agreement with previous reports [53,54].

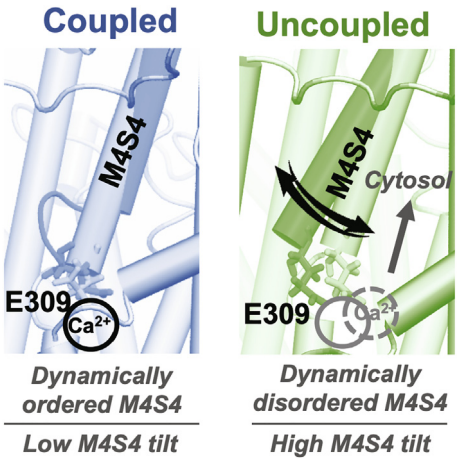

Fig. 7. Model of structural changes within the energy-transduction domain that induce SERCA uncoupling. SLN and $PLB_{26–52}$ shift the equilibrium of M4S4 from an ordered structural state (left) toward a state in which this domain is more tilted but also dynamically more disordered (right). We propose that this structural change perturbs Ca^{2+} occlusion in transport site II, thus facilitating Ca^{2+} slippage back to the cytosol.

4. Conclusion

In summary, we have tested the hypothesis that PLB's N-terminal phosphorylation domain is a primary contributor to the functional divergence among homologous SERCA regulators. Comparison between wild-type PLB and a PLB construct with a truncated N-terminal phosphorylation domain, $PLB_{26–52}$, showed no significant changes in the stability and orientation of the transmembrane domain, and also produces key intermolecular contacts and structural changes required for SERCA inhibition. Structural analyses showed that $PLB_{26–52}$, but not PLB_{WT}, induces changes in the orientation and dynamics of the energy-transduction domain M4S4 of SERCA that are similar to those induced by SLN, a protein analog that shares substantial homology with PLB but uncouples SERCA. We found that although these structural changes are weaker than those induced by SLN, the shift toward a dynamically disordered M4S4 helps explain the partial uncoupling of SERCA by $PLB_{26–52}$. Together, this mechanistic evidence indicates that the N-terminal phosphorylation domain of PLB is a primary contributor to the functional divergence among homologous SERCA regulators. Our MDS provides novel hypotheses that can be tested by functional mutagenesis studies or by additional simulations to determine how the energy landscapes and contact surfaces are shaped with changes in the M4S4 domain, and how these changes are allosterically transmitted to the catalytic elements of SERCA. Understanding how functional elements of SERCA effectors coevolve with regulation and operative divergence will be essential to fully appreciate the mechanisms of the SERCA regulation machinery.

CRediT authorship contribution statement

Eli Fernández-de Gortari: Investigation, Writing - review & editing. **Rodrigo Aguayo-Ortiz:** Investigation, Writing - review & editing. **Joseph M. Autry:** Writing - review & editing. **L. Michel Espinoza-Fonseca:** Conceptualization, Investigation, Writing - review & editing, Funding acquisition.

Declaration of Competing Interest

The authors declare that they have no known competing financial interests or personal relationships that could have appeared to influence the work reported in this paper.

Acknowledgments

This work was supported by the National Institutes of Health grant R01GM120142 (to L.M.E.-F.). This research was supported in part through computational resources and services provided by Advanced Research Computing at the University of Michigan, Ann Arbor.

Appendix A. Supplementary data

Supplementary data to this article can be found online at https://doi.org/10.1016/j.csbj.2020.02.016.

References

[1] Møller JV, Olesen C, Winther AM, Nissen P. The sarcoplasmic Ca2+-ATPase: design of a perfect chemi-osmotic pump. Q Rev Biophys 2010;43:501–66.

[2] Babu GJ, Bhupathy P, Carnes CA, Billman GE, Periasamy M. Differential expression of sarcolipin protein during muscle development and cardiac pathophysiology. J Mol Cell Cardiol 2007;43:215–22.
[3] Vangheluwe P, Schuermans M, Zador E, Waelkens E, Raeymaekers L, Wuytack F. Sarcolipin and phospholamban mRNA and protein expression in cardiac and skeletal muscle of different species. Biochem J 2005;389:151–9.
[4] Akin BL, Hurley TD, Chen Z, Jones LR. The structural basis for phospholamban inhibition of the calcium pump in sarcoplasmic reticulum. J Biol Chem 2013;288:30181–91.
[5] Toyoshima C, Iwasawa S, Ogawa H, Hirata A, Tsueda J, Inesi G. Crystal structures of the calcium pump and sarcolipin in the Mg2+-bound E1 state. Nature 2013;495:260–4.
[6] Winther AM, Bublitz M, Karlsen JL, Møller JV, Hansen JB, Nissen P, et al. The sarcolipin-bound calcium pump stabilizes calcium sites exposed to the cytoplasm. Nature 2013;495:265–9.
[7] Bal NC, Maurya SK, Sopariwala DH, Sahoo SK, Gupta SC, Shaikh SA, et al. Sarcolipin is a newly identified regulator of muscle-based thermogenesis in mammals. Nature Med 2012;18:1575–9.
[8] Mall S, Broadbridge R, Harrison SL, Gore MG, Lee AG, East JM. The presence of sarcolipin results in increased heat production by Ca(2+)-ATPase. J Biol Chem 2006;281:36597–602.
[9] Smith WS, Broadbridge R, East JM, Lee AG. Sarcolipin uncouples hydrolysis of ATP from accumulation of Ca2+ by the Ca2+-ATPase of skeletal-muscle sarcoplasmic reticulum. Biochem J 2002;361:277–86.
[10] Maurya SK, Bal NC, Sopariwala DH, Pant M, Rowland LA, Shaikh SA, et al. Sarcolipin is a key determinant of the basal metabolic rate, and its overexpression enhances energy expenditure and resistance against diet-induced obesity. J Biol Chem 2015;290:10840–9.
[11] Gamu D, Juracic ES, Fajardo VA, Rietze BA, Tran K, Bombardier E, et al. Phospholamban deficiency does not alter skeletal muscle SERCA pumping efficiency or predispose mice to diet-induced obesity. Am J Physiol Endocrinol Metab 2019;316:E432–42.
[12] Bal NC, Maurya SK, Singh S, Wehrens XH, Periasamy M. Increased reliance on muscle-based thermogenesis upon acute minimization of brown adipose tissue function. J Biol Chem 2016;291:17247–57.
[13] Autry JM, Thomas DD, Espinoza-Fonseca LM. Sarcolipin promotes uncoupling of the SERCA Ca2+ pump by inducing a structural rearrangement in the energy-transduction domain. Biochemistry-US 2016;55:6083–6.
[14] Sahoo SK, Shaikh SA, Sopariwala DH, Bal NC, Bruhn DS, Kopec W, et al. The N terminus of sarcolipin plays an important role in uncoupling sarco-endoplasmic reticulum Ca2+-ATPase (SERCA) ATP hydrolysis from Ca2+ transport. J Biol Chem 2015;290:14057–67.
[15] Kranias EG, Hajjar RJ. Modulation of cardiac contractility by the phospholamban/SERCA2a regulatome. Circ Res 2012;110:1646–60.
[16] Asahi M, McKenna E, Kurzydlowski K, Tada M, MacLennan DH. Physical interactions between phospholamban and sarco(endo)plasmic reticulum Ca2+-ATPases are dissociated by elevated Ca2+, but not by phospholamban phosphorylation, vanadate, or thapsigargin, and are enhanced by ATP. J Biol Chem 2000;275:15034–8.
[17] Bombardier E, Smith IC, Vigna C, Fajardo VA, Tupling AR. Ablation of sarcolipin decreases the energy requirements for Ca2+ transport by sarco(endo)plasmic reticulum Ca2+-ATPases in resting skeletal muscle. FEBS Lett 2013;587:1687–92.
[18] Mascioni A, Karim C, Barany G, Thomas DD, Veglia G. Structure and orientation of sarcolipin in lipid environments. Biochemistry-US 2002;41:475–82.
[19] Reddy LG, Jones LR, Cala SE, O'Brian JJ, Tatulian SA, Stokes DL. Functional reconstitution of recombinant phospholamban with rabbit skeletal Ca(2+)-ATPase. J Biol Chem 1995;270:9390–7.
[20] Espinoza-Fonseca LM, Autry JM, Thomas DD. Sarcolipin and phospholamban inhibit the calcium pump by populating a similar metal ion-free intermediate state. Biochem Biophys Res Commun 2015;463:37–41.
[21] Espinoza-Fonseca LM, Autry JM, Ramirez-Salinas GL, Thomas DD. Atomic-level mechanisms for phospholamban regulation of the calcium pump. Biophys J 2015;108:1697–708.
[22] Sheinerman FB, Honig B. On the role of electrostatic interactions in the design of protein-protein interfaces. J Mol Biol 2002;318:161–77.
[23] Singh DR, Dalton MP, Cho EE, Pribadi MP, Zak TJ, Seflova J, et al. Newly discovered micropeptide regulators of SERCA form oligomers but bind to the pump as monomers. J Mol Biol. 2019;431:4429–43.
[24] Olsson MHM, Sondergaard CR, Rostkowski M, Jensen JH. PROPKA3: consistent treatment of internal and surface residues in empirical pK(a) predictions. J Chem Theory Comput 2011;7:525–37.
[25] Sondergaard CR, Olsson MHM, Rostkowski M, Jensen JH. Improved treatment of ligands and coupling effects in empirical calculation and rationalization of pK(a) values. J Chem Theory Comput 2011;7:2284–95.
[26] Norimatsu Y, Hasegawa K, Shimizu N, Toyoshima C. Protein-phospholipid interplay revealed with crystals of a calcium pump. Nature 2017;545:193–8.
[27] Phillips JC, Braun R, Wang W, Gumbart J, Tajkhorshid E, Villa E, et al. Scalable molecular dynamics with NAMD. J Comput Chem 2005;26:1781–802.
[28] Weber W, Hünenberger PH, McCammon JA. Molecular dynamics simulations of a polyalanine octapeptide under ewald boundary conditions: influence of artificial periodicity on peptide conformation. J Phys Chem B 2000;104:3668–75.
[29] Darden T, York D, Pedersen L. Particle mesh Ewald: an N·log(N) method for Ewald sums in large systems. J Chem Phys 1993;98:10089–92.
[30] Essmann U, Perera L, Berkowitz ML. A smooth particle mesh Ewald method. J Chem Phys 1995;103:8577–93.
[31] Best RB, Zhu X, Shim J, Lopes PE, Mittal J, Feig M, et al. Optimization of the additive CHARMM all-atom protein force field targeting improved sampling of the backbone phi, psi and side-chain chi(1) and chi(2) dihedral angles. J Chem Theory Comput 2012;8:3257–73.
[32] Klauda JB, Venable RM, Freites JA, O'Connor JW, Tobias DJ, Mondragon-Ramirez C, et al. Update of the CHARMM all-atom additive force field for lipids: validation on six lipid types. J Phys Chem B 2010;114:7830–43.
[33] Fernandez-de Gortari E, Espinoza-Fonseca LM. Structural basis for relief of phospholamban-mediated inhibition of the sarcoplasmic reticulum Ca(2+)-ATPase at saturating Ca(2+) conditions. J Biol Chem 2018;293:12405–14.
[34] Espinoza-Fonseca LM, Ramirez-Salinas GL. Microsecond molecular simulations reveal a transient proton pathway in the calcium pump. J Am Chem Soc 2015;137:7055–8.
[35] El Hage K, Hedin F, Gupta PK, Meuwly M, Karplus M. Valid molecular dynamics simulations of human hemoglobin require a surprisingly large box size. Elife 2018;7:e45318.
[36] Gustavsson M, Verardi R, Mullen DG, Mote KR, Traaseth NJ, Gopinath T, et al. Allosteric regulation of SERCA by phosphorylation-mediated conformational shift of phospholamban. Proc Natl Acad Sci U S A 2013;110:17338–43.
[37] Hellstern S, Pegoraro S, Karim CB, Lustig A, Thomas DD, Moroder L, et al. Sarcolipin, the shorter homologue of phospholamban, forms oligomeric structures in detergent micelles and in liposomes. J Biol Chem 2001;276:30845–52.
[38] Pallikkuth S, Blackwell DJ, Hu Z, Hou Z, Zieman DT, Svensson B, et al. Phosphorylated phospholamban stabilizes a compact conformation of the cardiac calcium-ATPase. Biophys J 2013;105:1812–21.
[39] Kimura Y, Kurzydlowski K, Tada M, MacLennan DH. Phospholamban inhibitory function is activated by depolymerization. J Biol Chem 1997;272:15061–4.
[40] Trieber CA, Afara M, Young HS. Effects of phospholamban transmembrane mutants on the calcium affinity, maximal activity, and cooperativity of the sarcoplasmic reticulum calcium pump. Biochemistry-US 2009;48:9287–96.
[41] Reddy LG, Cornea RL, Winters DL, McKenna E, Thomas DD. Defining the molecular components of calcium transport regulation in a reconstituted membrane system. Biochemistry-US 2003;42:4585–92.
[42] Miyazawa S, Jernigan RL. Residue-residue potentials with a favorable contact pair term and an unfavorable high packing density term, for simulation and threading. J Mol Biol 1996;256:623–44.
[43] Kimura Y, Asahi M, Kurzydlowski K, Tada M, MacLennan DH. Phospholamban domain Ib mutations influence functional interactions with the Ca2+-ATPase isoform of cardiac sarcoplasmic reticulum. J Biol Chem 1998;273:14238–41.
[44] Schober P, Boer C, Schwarte LA. Correlation coefficients: appropriate use and interpretation. Anesth Analg 2018;126:1763–8.
[45] Inesi G, Ma H, Lewis D, Xu C. Ca2+ occlusion and gating function of Glu309 in the ADP-fluoroaluminate analog of the Ca2+-ATPase phosphoenzyme intermediate. J Biol Chem 2004;279:31629–37.
[46] Clausen JD, Bublitz M, Arnou B, Montigny C, Jaxel C, Møller JV, et al. SERCA mutant E309Q binds two Ca(2+) ions but adopts a catalytically incompetent conformation. EMBO J 2013;32:3231–43.
[47] Sun B, Stewart BD, Kucharski AN, Kekenes-Huskey PM. Thermodynamics of cation binding to the sarcoendoplasmic reticulum calcium atpase pump and impacts on enzyme function. J Chem Theory Comput 2019;15:2692–705.
[48] Raguimova ON, Smolin N, Bovo E, Bhayani S, Autry JM, Zima AV, et al. Redistribution of SERCA calcium pump conformers during intracellular calcium signaling. J Biol Chem 2018;293:10843–56.
[49] Espinoza-Fonseca LM, Colson BA, Thomas DD. Effects of pseudophosphorylation mutants on the structural dynamics of smooth muscle myosin regulatory light chain. Mol Biosyst 2014;10:2693–8.
[50] Kast D, Espinoza-Fonseca LM, Yi C, Thomas DD. Phosphorylation-induced structural changes in smooth muscle myosin regulatory light chain. Proc Natl Acad Sci U S A 2010;107:8207–12.
[51] Espinoza-Fonseca LM, Kast D, Thomas DD. Thermodynamic and structural basis of phosphorylation-induced disorder-to-order transition in the regulatory light chain of smooth muscle myosin. J Am Chem Soc 2008;130:12208–9.
[52] Glaves JP, Primeau JO, Espinoza-Fonseca LM, Lemieux MJ, Young HS. The phospholamban pentamer alters function of the sarcoplasmic reticulum calcium pump SERCA. Biophys J 2019;116:633–47.
[53] Asahi M, Sugita Y, Kurzydlowski K, De Leon S, Tada M, Toyoshima C, et al. Sarcolipin regulates sarco(endo)plasmic reticulum Ca2+-ATPase (SERCA) by binding to transmembrane helices alone or in association with phospholamban. Proc Natl Acad Sci U S A 2003;100:5040–5.
[54] Gorski PA, Glaves JP, Vangheluwe P, Young HS. Sarco(endo)plasmic reticulum calcium ATPase (SERCA) inhibition by sarcolipin is encoded in its luminal tail. J Biol Chem 2013;288:8456–67.
[55] Toyoshima C, Nakasako M, Nomura H, Ogawa H. Crystal structure of the calcium pump of sarcoplasmic reticulum at 2.6 A resolution. Nature 2000;405:647–55.
[56] Frank K, Tilgmann C, Shannon TR, Bers DM, Kranias EG. Regulatory Role of Phospholamban in the Efficiency of Cardiac Sarcoplasmic Reticulum Ca^{2+} Transport. Biochemistry 2000;39:14176–82. https://doi.org/10.1021/bi001049k.
[57] Karim CB, Marquardt CG, Stamm JD, Barany G, Thomas DD. Synthetic null-cysteine phospholamban analogue and the corresponding transmembrane domain inhibit the Ca-ATPase. Biochemistry 2000;39:10892–7.

[58] Kimura Y, Asahi M, Kurzydlowski K, Tada M, MacLennan DH. Phospholamban domain I/cytochrome b5 transmembrane sequence chimeras do not inhibit SERCA2a. FEBS Lett. 1998;425:509–12.
[59] Kimura Y, Kurzydlowski K, Tada M, MacLennan DH. Phospholamban regulates the Ca2+-ATPase through intramembrane interactions. J Biol Chem 1996;271:21726–31.
[60] Jones LR, Field LJ. Residues 2-25 of phospholamban are insufficient to inhibit Ca^{2+} transport ATPase of cardiac sarcoplasmic reticulum. J Biol Chem 1993;268:11486–8.
[61] Sasaki T, Inui M, Kimura Y, Kuzuya T, Tada M. Molecular Mechanism of Regulation of Ca^{2+} Pump ATPase by Phospholamban in Cardiac Sarcoplasmic Reticulum. Effects of Synthetic Phospholamban Peptides on Ca^{2+} Pump ATPase. J Biol Chem 1992;267:1674–9.
[62] Ahmed Z, Reid DG, Watts A, Middleton DA. A solid-state NMR study of the phospholamban transmembrane domain: local structure and interactions with Ca^{2+}-ATPase. Biochim Biophys Acta 2000;1468:187–98.